

FRNC- R- 24

NOTICE 1980

ICNF

INIC

NSA

2

Elastic Scattering of Tritons by ^{16}O

M. WERY

Laboratoire des Basses Energies

C.R.N. and U.L.P. BP 20/CR 67037 Strasbourg Cedex

Abstract : Angular distributions and excitation functions have been measured for the $^{16}\text{O}(t,t)$ reaction from 1.4 to 3.7 MeV triton energy using a differentially pumped gas target. The observed resonances have been analysed with the Humblet-Rosenfeld theory. It appears that the 13-15 MeV excitation range of the compound system of ^{19}F is dominated by several levels of large triton partial width. Levels populated in the three-particle transfer reaction ($^7\text{Li},\alpha$) on ^{16}O are compared with the resonances.

E

NUCLEAR REACTION $^{16}\text{O}(t,t)$, $E = 1.4 - 3.7$ MeV ; measured σ
(E_t , $\theta_{\text{lab}} = 30^\circ, 60^\circ, 70^\circ, 90^\circ, 120^\circ, 140^\circ, 150^\circ, 160^\circ$) ; $E = 1.85$;
2.0 ; 2.44 ; 2.66 ; 3.0 ; 3.24 ; 3.34 ; 3.70 MeV ; measured $\sigma(E_t, \theta)$;
 ^{19}F deduced levels $L, J, \pi, \Gamma_t, \Gamma$. Natural gas target.

1. Introduction

It is shown from many recent results that nuclear states in high excitation regions may have relatively simple structure, allowing them to stand out from the statistical background. This is the case, especially, of the excited states at the beginning of the (2s-1d) shell observed through resonant scattering or populated preferentially in transfer reactions ¹⁾ .

In this experiment the reaction $^{16}\text{O}(t,t)$ was studied in order to extend our understanding of the compound system ^{19}F at high excitation energies. The resonant behaviour of the excitation functions of the elastic scattering was observed by Etoh et al ²⁾ in the same energy range and Pullen et al ³⁾ had suggested that a resonance with a large triton partial width could be located at high excitation in ^{19}F . New measurements are reported and analysed in the present work from 13 up to 15 MeV.

2. Experimental procedure

The tritons were accelerated by the 3 MeV Strasbourg Van de Graaff. The beam was collimated by a magnetic quadrupole doublet. The beam angular dispersion was reduced to $\pm 6'$ by two slits before reaching the scattering chamber. The current intensity on target was generally 100 nA, with a mean transmission factor of 70 %. The energy was calibrated through

the analysing magnet using the threshold of the reaction ${}^7\text{Li}(p,n){}^7\text{Be}$.

In order to measure accurately the reaction cross sections, a scattering chamber for gaseous targets was built. This type of target is perfectly homogeneous, not easily contaminated and does not deteriorate under bombardment. The continuous monitoring of the thickness is easy and the atom density is, to a good approximation, a known function of pressure and temperature. As oxygen is naturally gaseous and available with high chemical and isotopic purity, a two-stage differentially pumped system, which does not spoil the energy resolution of the beam, was used. For a pressure usually fixed at one torr, the consumption of oxygen did not exceed 1 l.atm/h. The description of the scattering chamber and its characteristics, as well as the measurements of beam current, pressure and temperature, and the detection geometry are given in detail in a previous paper ⁴⁾.

Surface barrier semi-conductor detectors were used. A typical spectrum of particles emitted at 149.04° from the bombardment of an ${}^{16}\text{O}$ target by 3.2 MeV tritons is shown in fig. 1. The overall resolution is about 20 keV (fwhm) : it is essentially the intrinsic resolution of the detectors. The separation of the p_5 and a_6 groups is 40 keV. It can be seen that neither contamination nor background are present.

The accuracy of these measurements has been estimated using different methods ^{4,5)}. In one of them, the experimental cross sections values were compared to Rutherford scattering ones for the case of 1 MeV protons on ${}^{40}\text{Ar}$. The observed deviations over a wide angular range and

under good statistical conditions never exceeded 5 %. This is also the resultant of all the uncertainties which were considered in this work ; The accuracy is worse when the cross section is very small or when it is difficult to separate a peak.

3. Results and analysis

3.1. EXPERIMENTAL RESULTS

Excitation functions for the reaction $^{16}\text{O}(t,t)$ have been measured at laboratory angles of 30.95° , 60.32° , 70.20° , 90° , 119.67° , 139.33° , 149.04° and 158.52° over the incident triton energy range 1.4 - 3.7 MeV. The energy steps, usually 20 keV, were reduced to 10 keV in sensitive regions. As can be seen in fig. 2, strong correlations are observed between the resonant structures at all backward angles where nuclear effects should dominate. Whenever comparisons between the present measurements and those of Etch²⁾ were possible, excellent agreement was noted. These measurements were completed with angular distributions recorded at energies corresponding to the extrema in the excitation curves, namely, 1.85, 2., 2.44, 2.66, 3., 3.24, 3.34 and 3.37 MeV over an angular range from 20° to 165° in steps of 5° . For angles smaller than 70° it was not possible to separate the triton group from p_3 and α_6 . We therefore give the sum of these three contributions, under the assumption that the α_6 and p_3 channels are negligible compared to the triton group. This is always clearly the case at 90°_{lab} where the three peaks are well resolved.

On the other hand, for angles greater than 70° , whenever other peaks overlapped the elastic peak, the data points were rejected.

The calculations of the absolute cross sections and of their quadratic errors were performed with the aid of the acquisition and analysis system ATRAIT ⁶⁾. The experiments may be essentially monitored in real time, allowing data points to be measured again immediately if necessary.

3.2. FORMALISM

3.2.1. Parametrization of the collision matrix elements (ref. ⁷⁾).

We used the following parametrization of the elements of the collision matrix $U_{c',c}$ between the channels c, c' :

$$U_{c',c} = \exp(i[\omega_{c'} + \phi_{c'}]) \exp(i[\omega_c + \phi_c]) \left\{ \delta_{cc'} + (k_c k_{c'} P_{c'} P_c)^{1/2} \times \right. \\ \left. \left[Q_{cc'}(E) - i \sum_{n=1}^{n_{\max}} \frac{\exp(i\xi_{c'n}) \exp(i\xi_{cn}) X_{c'n}^{1/2} X_{cn}^{1/2}}{e^{-\epsilon_n}} \right] \right\} \quad (1)$$

The elements $U_{c',c}$ are also characterized by J^M , but since the total angular momentum J and its projection M are conserved, they have been omitted to simplify the notation.

The two body channel and its associated quantum numbers (s, ℓ) are specified by the index c .

$$\text{The quantities } \omega_c = \sum_{j=1}^{\ell} \text{arctg } \eta/j \quad (2)$$

and

$$\phi_c = -\text{arctg} \left(\frac{P_c}{C_c} \right) \quad (3)$$

$\frac{P_c}{C_c} = a_c$

are Coulomb and hard sphere phases, respectively ; n is the Coulomb parameter.

The quantity X_{cn} is defined by
$$X_{cn} = \frac{\Gamma_{cn}}{K_{cn}} \left| O_{cn}^2 \right| \quad (4)$$

with
$$O_{cn} = G_{cn} + i\Gamma_{cn} \quad (5)$$

and Γ_{cn} is the total width ; ξ_{cn} is the real part of the resonant phase.

The wave number $k_{cn} = K_{cn} - i\gamma_{cn}$ (6)

is associated with the pole ϵ_n .

The continuous background Q is replaced by a complex constant

$$R_{\ell J} \exp(i\theta_{\ell J}).$$

The penetrability factor is expressed in Coulomb functions as

$$P_c = \frac{1}{(\mathbb{R}_c^2 + G_c^2) r_c = a_c} \quad (7)$$

It can be noted that the parameter r_c only enters into $U_{c,c}$ through the Coulomb functions; therefore the characteristics of the resonance are independent of radius.

3.2.2. Cross section formula

The study of the scattering of unpolarized spin 1/2 particle on a spin 0 target ($c = c'$; $\delta_{c,c} = 1$; $J = \ell \pm 1/2$; $\pi = (-1)^\ell$) leads to the differential cross section :

$$\frac{d\sigma}{d\Omega} = \left| g(\theta) \right|^2 + \left| h(\theta) \right|^2 \quad (8)$$

The amplitudes $g(\theta)$ and $h(\theta)$ are expressed as functions of the collision

matrix elements

$$U_{\ell}^{+} = U^{J=\ell+s} \quad (9)$$

and

$$U_{\ell}^{-} = U^{J=\ell-s} \quad (10)$$

as follows :

$$g(\theta) = -\frac{1}{2k \sin^2 \theta/2} \exp(-2i \ln \sin \theta/2) + \frac{1}{2ik} \sum_{\ell=0}^{\ell_{\max}} \left\{ (\ell+1) U_{\ell}^{+} + \ell U_{\ell}^{-} - (2\ell+1) \exp(2i\delta_{\ell}) P_{\ell}(\cos \theta) \right\} \quad (11)$$

$$h(\theta) = \frac{1}{2k} \sum_{\ell=0}^{\ell_{\max}} (U_{\ell}^{+} - U_{\ell}^{-}) P_{\ell}^1(\cos \theta) \quad (12)$$

The quantities P_{ℓ} and P_{ℓ}^1 are the Legendre polynomials and the associated Legendre functions.

3.3. ANALYSIS

A program written by L. Kraus ⁸⁾ which calculates the elements of the collision matrix according to this above formalism was used. The fit between the theoretical and experimental curves is obtained by a minimization of X^2 .

- It was noted by the study of the penetrability P_{ℓ} and phase factors δ_{ℓ} as a function of triton energy (fig. 2) that only partial waves with ℓ value no larger than 3 contribute significantly to the scattering cross sections. The maximum angular momentum was therefore chosen to be 3.

A search was then made for parameters which produced satisfactory agreement between experimental and theoretical values by visual comparison and χ^2 minimization. The initial sample was then extended by adding points belonging to a neighbouring structure. The ℓ value, the width and the energy of the additional resonance were fixed as above. A new search for the best parameters could then be performed, using a multi-level formalism in which the parameters for the initial sample remain fixed. A new starting set was thus obtained, to which more data could be added. We have proceeded in this way until the whole final sample was included. However, this relatively simple method did not give a good fit in the region near 13.25, 14.30 and 14.50 MeV ; in the neighbourhood of those energies we had to introduce one additional resonance. An excellent agreement was then obtained (See fig. 4). The parameters for this fit are listed in table 1. Although the agreement is good, since several resonances overlap, the original sets of parameters were changed several times to make sure, first that the fitting program was not trapped in a local minimum of χ^2 and second, that the final parameter set is unique. These last considerations give the limits of this method taking into account our hypothesis and our experimental errors. Table 1 includes estimates of these uncertainties. Finally, it is to be noted that no success could be obtained in producing a comparable fit starting with different initial samples and other ℓ values for the resonances.

In table 1, except for the s-wave resonances, the total angular momenta are not uniquely determined. With the mutual influence between some neighbouring resonances and such low values of angular momentum ($\ell \leq 2$), it seems hard to distinguish between the values $J = \ell \pm 1/2$ for a given ℓ value.

The maximum triton energy dispersion was estimated to be less than 5 keV. This is also the smallest energy step which was used for several experimental points measured in the neighbourhood of 1.625 MeV : for this reason only an upper limit is given for the total width of the s-wave resonance at $E_x \approx 13.067$ MeV. Finally, because of the upper incident-energy limit, the characteristics of the two highest excited states were determined using a reduced sample.

4. Discussion and conclusions

It seems clear that the Humblet-Rosenfeld multilevel formalism is appropriate for analysing the elastic scattering reaction $^{16}\text{O}(t,t)$. Moreover, we never had to include a continuous background Q which is often introduced to take into account effects due to direct reaction mechanisms. The 13 to 14.5 MeV region of excitation of ^{16}O is dominated by eleven levels, most of which have not only a large total width but also a substantial partial width for tritons.

In order to obtain additional informations from the elastic scattering, results for the reaction channels were simultaneously extracted, as indicated on fig. 1. The integrated cross sections from 20° to 160° for each reaction show some of the structures observed in the excitation curves (as we have already shown for the α_0 channel ⁹⁾), but we have been unable to establish definite correlations between the different channels. This phenomenon was previously observed at lower energy by Kobzev et al ¹⁰⁾. Moreover in comparing the average values of the cross

sections, it appears that no reaction channel is significantly stronger than the others.

These observations are in good agreement with other results from reactions leading to the same excitation region in ^{19}F , namely, by proton bombardment of ^{18}O target at energies above 5 MeV. Excitation curves of the (p,p), (p,n) and (p, α) reactions on ^{18}O at energies above 5 MeV also show very complicated structures. In a recent analysis of (p,p) elastic scattering, Orihara et al. ¹¹⁾ report three $T = 1/2$ resonances in ^{19}F at 13.035, 13.080 and 13.321 MeV whose spins are $5/2^+$, $7/2^+$ and $7/2^-$ respectively; the ratios Γ_p/Γ vary from 18 to 33 %.

In collaboration with a Saclay group ¹⁵⁾ we have studied three-particle transfer on ^{16}O via the reaction $^{16}\text{O}(^7\text{Li},\alpha)^{19}\text{F}$. This reaction has also been studied by Glukhov et al. ¹²⁾ who report the presence of pronounced structures in the neighbourhood of the ($^{16}\text{O}+\text{t}$) threshold. According to the authors, these results confirm the predictions of the threshold-states theory of Bas ¹³⁾. Fig. 5 shows a typical spectrum obtained ^{5,15)} with a better resolution than that of reference ¹²⁾. In the region of excitation corresponding to our ($^{16}\text{O}+\text{t}$) results, four structures were found at all angles, which are among the most intense in these spectra even though they are superimposed on the "break-up" peak. By simple and direct comparison, they show widths of the same order as those found in the elastic channel, within experimental uncertainties (See table 2). All the resonances have positive parity and an large triton partial width. In addition, in the low energy portion of the ^{19}F excitation spectrum, the members of the ground state $K = 1/2^+$ rotational band [(sd)³ configurations] are preferentially populated by the reaction

(${}^7\text{Li}, \alpha$). Preliminary angular distributions of these states show forward peaking as in the case of the other low-lying strongly-populated levels ¹²⁾. In the direct transfer hypothesis, the angular momentum matching conditions for the entrance and exit channels favour levels with small values of spin in this ${}^{19}\text{F}$ excitation region : these predictions are not in contradiction with our elastic scattering results. Many levels are expected at such a high excitation ; the selection of only some of them by the two types of reactions we have studied (triton elastic scattering and transfer) suggests that they possess a relatively simple configuration. Unfortunately, the present lack of microscopic calculations and of additional experimental information, especially from scattering and transfer of three particles on ${}^{16}\text{O}$ above 15 MeV in ${}^{19}\text{F}$, does not allow us to look for the presence of a new rotational band nor to explain the configurations of such states without formulating new hypothesis.

The author wishes to thank Professor D. Magnac-Valette for her support and encouragement of this work and Professor E. Cotton for providing him the opportunity of performing the transfer study in Saclay with G. Bassani, A. Foti and N. Saunier. He also thanks C. Gerardin for his participation in the transfer experiments, and V. Gillet and A. Zuker for very helpful discussions and comments.

TABLE 1

Resonance parameters used in the calculation of the theoretical curves of fig. 4.

$E_{c.m.}$ (keV)	E_x (keV)	ℓ	J^π	$\Gamma_{c.m.}$ (keV)	$\Gamma_t/(100\Gamma)$
1368	13067 ± 4	0	$1/2^+$	$\Gamma \leq 10$	
1545	13244 ± 10	1	$1/2^-$	77	30
1570	13269 ± 10	0	$1/2^+$	4.5	5.5
1832	13531 ± 10	0	$1/2^+$	22	13.5
2018	13717 ± 20	1	$3/2^-$	128	37
2178	13877 ± 15	0	$1/2^+$	101	42
2447	14144 ± 20	0	$1/2^+$	21	4.5
2555	14250 ± 15	2	$3/2^+$	51	36
2652	14351 ± 10	0	$1/2^+$	154	65
2759	14458 ± 25	1	$3/2^+$	179	38
2763	14462 ± 25	2	$5/2^+$	46	18.5

TABLE 2

Comparison of states populated by the $^{16}_0(^7\text{Li},\alpha)^{19}\text{F}$ and $^{16}_0(t,t)^{16}_0$ reactions in the region $13 < E_x < 14.5$ MeV.

E_x (keV) a)	E_x (keV) b)	ℓ b)	J^π b)	$\Gamma_c/(100\tau)$ b)
12900 \pm 50				
13460 \pm 50	13531 \pm 10	0	1/2 ⁺	13.5
13940 \pm 50	13877 \pm 15	0	1/2 ⁺	42
14300 \pm 50	14250 \pm 15	2	3/2 ⁺	36
	14351 \pm 10	0	1/2 ⁺	65

a) From the $^{16}_0(^7\text{Li},\alpha)^{19}\text{F}$ reaction at $E_{\text{Li}} = 30$ MeV ^{5,15)}

b) From the elastic scattering of tritons by $^{16}_0$.

REFERENCES

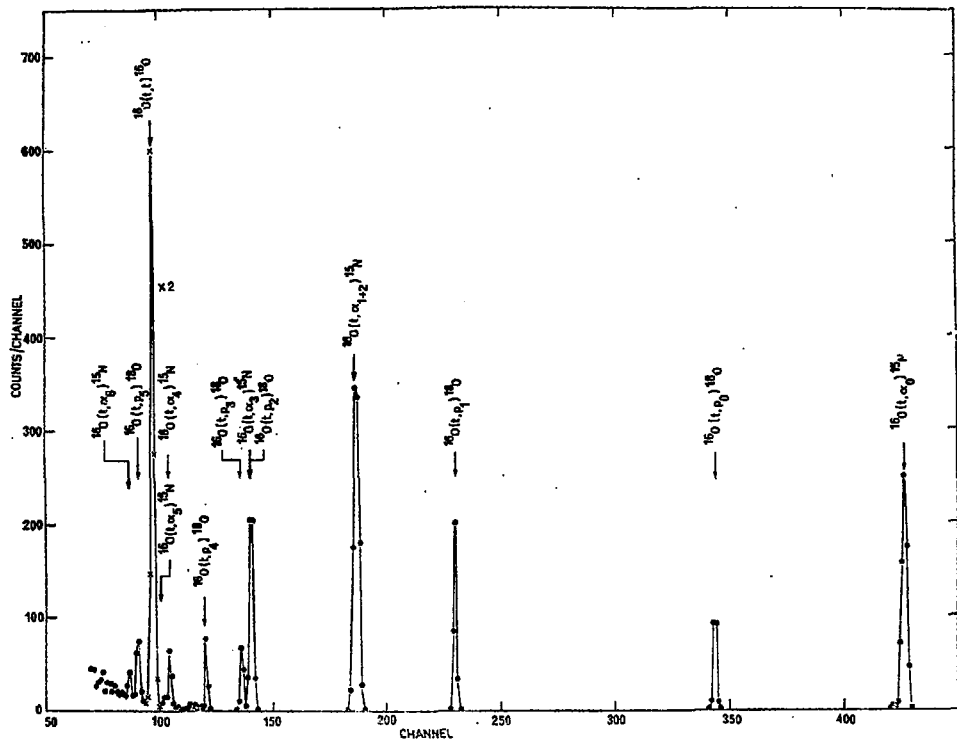
1. Proceedings of the symposium on heavy ion reactions and many particle excitations, Saclay, 1971, J. Phys. (Paris), Suppl. 32, C6 (1971) ; European Conference on nuclear physics, Aix en Provence, 1972, J. Phys. (Paris), 33, C5 (1972)
2. K. Etoh, N. Kawai, Y. Matsuda and T. Murata, J. Phys. Soc. Japan 24 (1968) 422
3. D.J. Pullen, J.R. Rook and R. Middleton, Nucl. Phys. 51 (1964) 88
4. M. Wery and F. Riehl, Nucl. Instr. 96 (1971) 425
5. M. Wery, Thèse, Strasbourg, 1972
6. M. Wery, P. Wittmer, J.B. Bueb and C. Ring, Nucl. Instr. 96 (1971) 309
7. J. Humblet and L. Rosenfeld, Nucl. Phys. 26 (1961) 529 ; J. Humblet, Nucl. Phys. 50 (1964) 1 ; Fundamentals in nuclear theory (IAEA, Vienna, 1967) 369
8. L. Kraus, Thèse, Strasbourg, 1971
9. M. Wery, Thèse 3e cycle, Strasbourg, 1965 ; C. Garardin, M. Wery, R. Seltz and D. Magnac-Valette, Compt. Rend. 261 (1965) 1512
10. A.P. Kobzev, A.V. Gromov, K. Kashlik, K. Nekvedyuk, V.I. Salatskii and S.A. Tělezchnikov, Yad. Fiz. 5 (1967) 510
11. H. Orihara, G. Rudolf and Ph. Gorodetzky, Nucl. Phys. A203 (1973) 78
12. Yu.A. Glukhov, B.G. Novatskii, A.A. Ogloblin, S.B. Sakuta and D.N. Stepanov, Izv. Akad. Nauk. SSSR (Ser. Fiz.) 33 (1969) 609.
13. A.I. Baz, Phil. Mag. 8 (1959) 349 ; A.I. Baz and V.I. Manko, Phys. Lett. 28 (1969) 541 ; A.I. Baz and V.I. Manko, Sov. J. Nucl. Phys. 10 (1970) 46

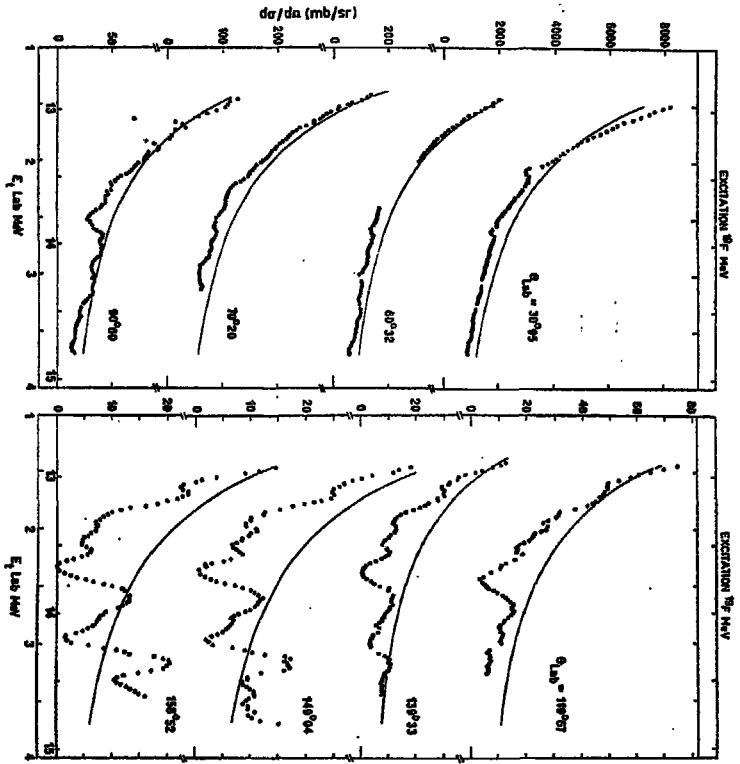
14. G. Bassani, L. Bianchi, A. Cunsolo, R. Dondelle, M. Daury, F. Jusczak, R. Langlois, J.P. Meurgues, B. Pierre, N. Saunier and M. Wery, Comptes Rendu Saclay C.E.A. -N- 1522 (1971) 61

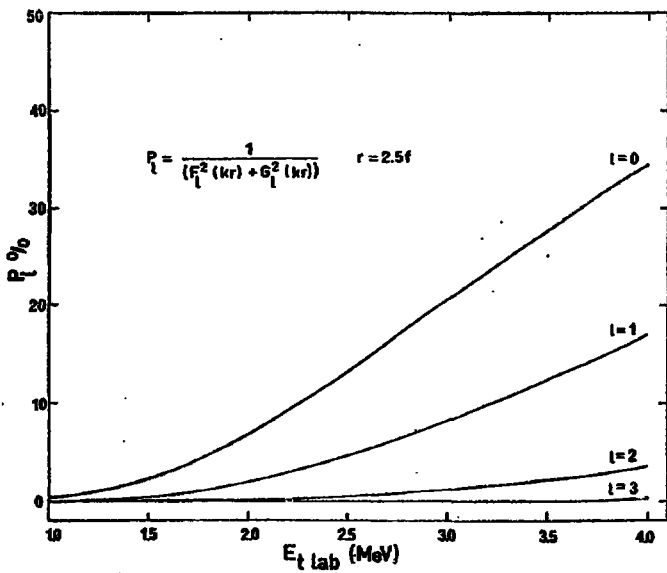
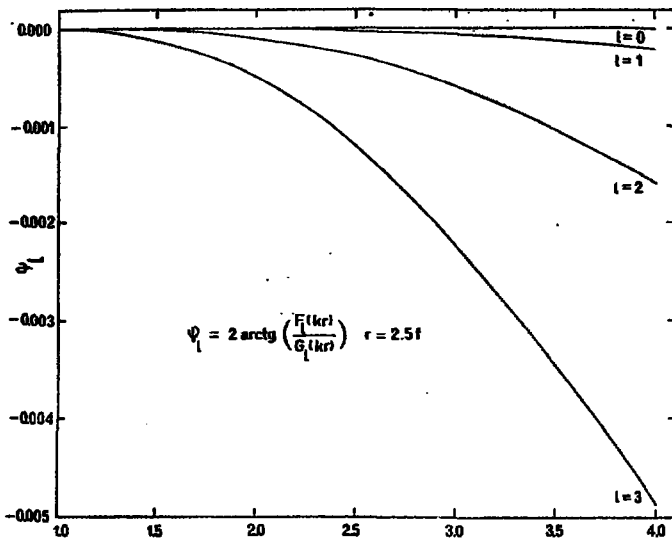
15. G. Bassani, A. Foti, C. Gerardin, N. Saunier and M. Wery, Suppl. J. Phys. (Paris) 33 CS (1972) 68.

FIGURE CAPTIONS

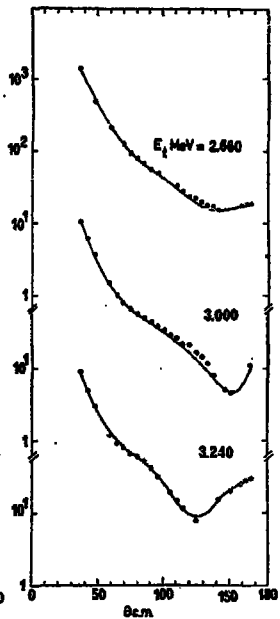
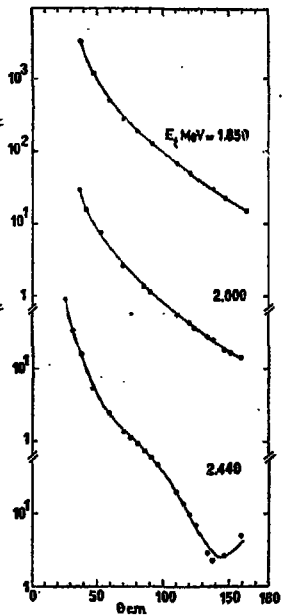
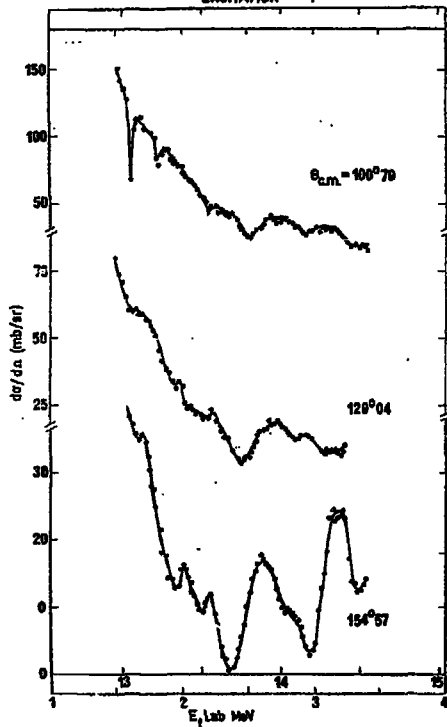
- Fig. 1. Typical charged particle spectrum from the bombardment of ^{16}O by tritons : $E_t = 3.200$ MeV, $\theta_{\text{lab}} = 149.04^\circ$.
- Fig. 2. The $^{16}\text{O}(t,t)^{16}\text{O}$ differential cross section (lab system) versus lab bombarding energy and excitation energy of ^{19}F . The solid curves are calculated Rutherford cross sections. The dots are experimental data. The uncertainties of the data are discussed in the text.
- Fig. 3. The penetrabilities and the "hard sphere" phases of the $^{16}\text{O}(t,t)^{16}\text{O}$ channel versus lab bombarding energy.
- Fig. 4. The $^{16}\text{O}(t,t)^{16}\text{O}$ differential cross section (c.m. system) versus lab bombarding energy and excitation energy of ^{19}F and versus $\theta_{\text{c.m.}}$. The solid curves are the theoretical calculations using the resonance parameters given in table 1. The dots are experimental data.
- Fig. 5. Typical spectrum for the $^{16}\text{O}(^7\text{Li},\alpha)^{19}\text{F}$ reaction : $E_{\text{Li}^7} = 30$ MeV, $\theta_{\text{lab}} = 12^\circ 36'$.







EXCITATION ^{19}F



Handwritten mark

$O^{16} (Li^7, \alpha) F^{19}$

$\theta_{lab} = 12^{\circ}36'$

$E_{Li^7} = 30 \text{ Mev}$

